

Electronic structure of metallic antiperovskite compound GaCMn₃

J. H. Shim, S. K. Kwon, and B. I. Min

Department of Physics, Pohang University of Science and Technology, Pohang 790-784, Korea
(February 1, 2008)

We have investigated electronic structures of antiperovskite GaCMn₃ and related Mn compounds SnCMn₃, ZnCMn₃, and ZnNMn₃. In the paramagnetic state of GaCMn₃, the Fermi surface nesting feature along the ΓR direction is observed, which induces the antiferromagnetic (AFM) spin ordering with the nesting vector $\mathbf{Q} \sim \Gamma R$. Calculated susceptibilities confirm the nesting scenario for GaCMn₃ and also explain various magnetic structures of other antiperovskite compounds. Through the band folding effect, the AFM phase of GaCMn₃ is stabilized. Nearly equal densities of states at the Fermi level in the ferromagnetic and AFM phases of GaCMn₃ indicate that two phases are competing in the ground state.

PACS numbers: 71.18.+y; 71.20.-b; 75.10.-b

Due to recent observations of giant-magnetoresistance (GMR) phenomenon in GaCMn₃ [1,2] and superconductivity in MgCNi₃ [3], compounds with antiperovskite structure have attracted great attention. Especially, antiperovskite manganese compounds that exhibit intriguing magnetic structures have been studied intensively [4–7]. Although the antiperovskite structure has an analogy to the perovskite oxides, their physical properties are very different. The antiperovskite structure locates transition metal elements at the octahedral corners, not at the centers. For example, in the antiperovskite GaCMn₃, C is centered in the octahedron composed of six Mn atoms, and Mn has only two nearest neighbor C atoms in contrast to the perovskite oxides in which a transition metal has six nearest neighbor oxygens.

GaCMn₃ exhibiting the GMR phenomenon has the antiferromagnetic (AFM) phase in the ground state [4]. Spins located on the (111) plane are ferromagnetically coupled and polarized collinearly along the [111] direction. The spin directions in these ferromagnetic (FM) planes are alternating along the [111] direction to have the AFM phase. Upon heating, it shows a first order transition to the FM phase at the transition temperature $T_t \sim 160$ K through a small region of the intermediate state where both the AFM and FM components are present [1,2]. T_t decreases with increasing magnetic field or pressure [8]. The transition is accompanied by the discontinuous suppression of volume and resistivity. The GMR phenomenon is manifested in this region. T_t also depends on the C stoichiometry. That is, with small deficit of C ($\sim 4\%$), T_t is reduced to 0 K and the AFM region disappears [5]. GaCMn₃ has the Curie temperature of $T_C \sim 250$ K. The magnetic moment per Mn is $\mu_{\text{Mn}} = 1.8 \pm 0.1 \mu_B$ at 4.2 K in the AFM phase, and $\mu_{\text{Mn}} = 1.3 \pm 0.1 \mu_B$ at 193 K in the FM phase [5]. On the other hand, the recent neutron diffraction study shows that $\mu_{\text{Mn}} \sim 1 \mu_B$ for both phases [2]. The relatively small magnetic moment, as compared to other manganese intermetallic compounds, reflects that this system would be described by the itinerant magnetism.

The spin configuration and the magnetic structure vary in a complicated way by electron or hole doping in the Mn

antiperovskite system [6]. For effectively one-hole doped ZnCMn₃, the spin configuration becomes non-collinear with the tetragonal magnetic structure, and the AFM and FM phases coexist in the ground state [7]. This coexisting phase is similar in nature to the intermediate phase observed in GaCMn₃ [1]. There is a first order transition to the FM phase with $T_C \sim 350$ K. Carbon deficient GaC_{0.935}Mn₃ also has a similar magnetic structure to ZnCMn₃. For effectively one-electron doped SnCMn₃, the spin configuration is also non-collinear up to $T_C \sim 290$ K with a complicated magnetic structure. Differently from the above compounds, SnCMn₃ does not have a stable FM phase. On the other hand, ZnNMn₃ which has the same number of valence electrons as GaCMn₃ shows different magnetic structure and properties [9]. It also has an AFM phase in the ground state, but no stable FM phase at higher temperature. Upon heating, it shows a direct transition from the AFM to the paramagnetic (PM) phase. Moreover, the AFM phase itself shows a different magnetic configuration. Spins on the (111) plane are non-collinear with clockwise or counterclockwise spin current configurations, and so the spin moments in the plane are compensating each other. Spin current directions in such (111) planes, that is, the spin chiralities are alternating along the [111] direction [5]. The origin of such intriguing magnetic structures in antiperovskite Mn compounds has not been addressed yet.

In this paper, we have studied electronic structures of GaCMn₃ and related antiperovskite Mn compounds such as ZnCMn₃, SnCMn₃, and ZnNMn₃. Band structures in their PM phases indicate that the magnetic structures are strongly correlated with the Fermi surface nesting. To investigate the correlation between the magnetic structure and the Fermi surface nesting, we have evaluated the susceptibility, and discussed the doping effects on the susceptibility and the magnetic structure. We have also studied the electronic structures of both AFM and FM phases of GaCMn₃ and compared them with that of the PM phase.

We have used the linearized muffin-tin orbital (LMTO) band method in the local spin density approximation (LSDA). We include the valence band muffin-tin orbitals

up to d for Ga and Mn, p for C. Ga $3d$ state is considered as core state. We consider the cubic structure with lattice constant $a = 3.89 \text{ \AA}$ for all magnetic structures of GaCMn_3 . In reality, the AFM phase of GaCMn_3 has slightly larger lattice constant than the FM phase by about 0.1 % near the transition temperature [2]. However, such a small difference in the lattice constant gives minor effect on the electronic structure. For the calculation of AFM structure, we have considered a doubled unit cell along the $[111]$ direction which is trigonal. Atomic sphere radii of Ga, C, and Mn are employed as 1.5, 0.8, 1.4 \AA , respectively. To evaluate susceptibilities, we have also obtained electronic structures of related compounds, SnCMn_3 , ZnCMn_3 , and ZnNMn_3 , with lattice constants 3.99, 3.93, 3.89 \AA , respectively [6,9]. Because Zn $3d$ state is located near E_F , it is treated as valence band. The other structural parameters are the same as in the case of GaCMn_3 .

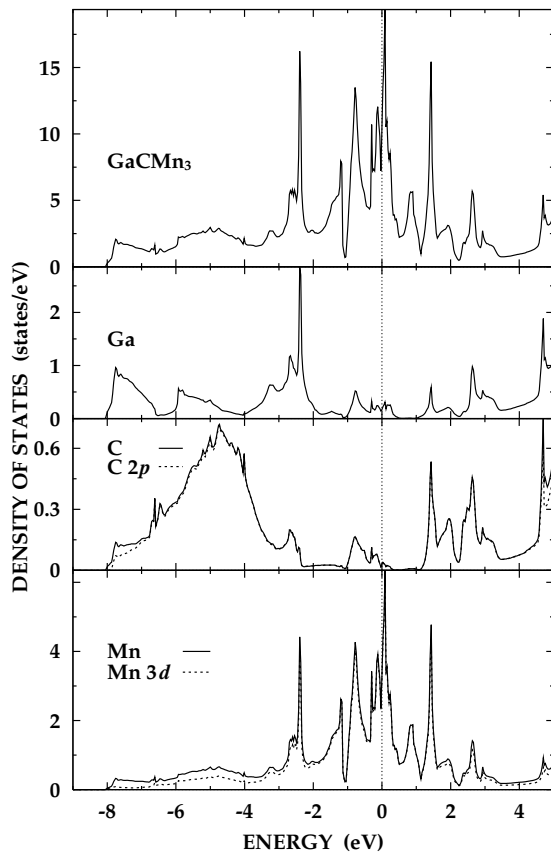


FIG. 1. The total and atomic site projected local DOSs of GaCMn_3 in the PM phase. The DOS peak near -12 eV which is mainly composed of C $2s$ state is not shown.

Figure 1 shows the total density of states (DOS) and projected local density of states (PLDOS) of GaCMn_3 in its PM phase. There exists strong hybridization between Mn $3d$ and two neighboring C $2p$ states, which gives rise to the extended bonding states between -3 eV and -7 eV . Due to this hybridization, the band width of

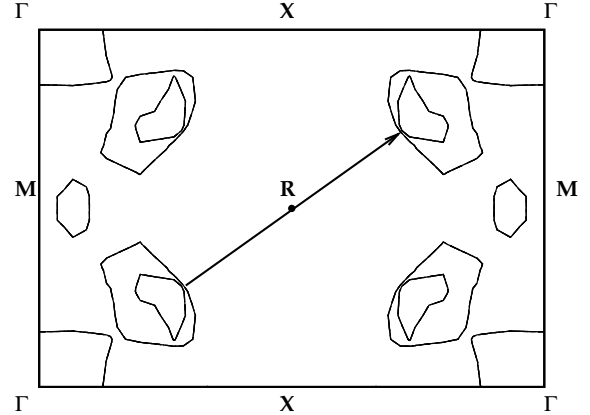


FIG. 2. The Fermi surface of GaCMn_3 on the (110) plane of the simple-cubic BZ. The arrow corresponds to the nesting vector \mathbf{Q} along the $[111]$ direction.

Mn $3d$ states becomes wide so that the system behaves as an itinerant electron system. At the Fermi level E_F , Mn $3d$ nonbonding states are located, and so the DOS at E_F is mainly due to Mn $3d$ states.

Band structure of GaCMn_3 indicates that three bands cross the Fermi level, forming the Fermi surfaces roughly consistent with Ref. [10]. Figure 2 provides the Fermi surfaces in the (110) plane of the simple-cubic Brillouin zone (BZ). Noteworthy is the nesting feature along the $[111]$ direction, which is expected to be closely related to the AFM ground state of GaCMn_3 . The size of the nesting vector is $\mathbf{Q} = \frac{9}{10}\Gamma\text{R}$. It thus reflects that the Fermi surface nesting would induce the spin ordering along the $[111]$ direction with wave vector $\mathbf{Q} \sim \Gamma\text{R}$, resulting in the AFM structure observed in GaCMn_3 .

In order to examine the nesting feature more clearly, we have evaluated the susceptibility which would drive the magnetic instability. The bare electronic susceptibility χ_0 can be obtained using the band structure output [11]:

$$\chi_0(\mathbf{q}) = \frac{1}{N} \sum_{n,n',\mathbf{k}} \frac{f(\epsilon_{n,\mathbf{k}})[1 - f(\epsilon_{n',\mathbf{k}+\mathbf{q}})]}{\epsilon_{n',\mathbf{k}+\mathbf{q}} - \epsilon_{n,\mathbf{k}}}, \quad (1)$$

where $f(\epsilon)$ is the Fermi-Dirac distribution function, $\epsilon_{n,\mathbf{k}}$ and $\epsilon_{n',\mathbf{k}+\mathbf{q}}$ are the eigenvalues at \mathbf{k} and $\mathbf{k}+\mathbf{q}$ of the first BZ with the band indices n and n' . Some ordering such as charge or spin density wave is induced with wave vector \mathbf{Q} which maximizes $\chi_0(\mathbf{Q})$. In this system, we have considered only three bands crossing the Fermi level to obtain the susceptibility.

Figure 3 shows the calculated susceptibilities of GaCMn_3 and related compounds, SnCMn_3 , ZnCMn_3 , and ZnNMn_3 . In the susceptibility of GaCMn_3 , local maxima are observed at point Γ and near point R. This feature suggests that the FM phase with $\mathbf{Q} = 0$ or the AFM phase with $\mathbf{Q} \sim \Gamma\text{R}$ would be stabilized depending on the situation. The \mathbf{k} point denoted by vertical arrow

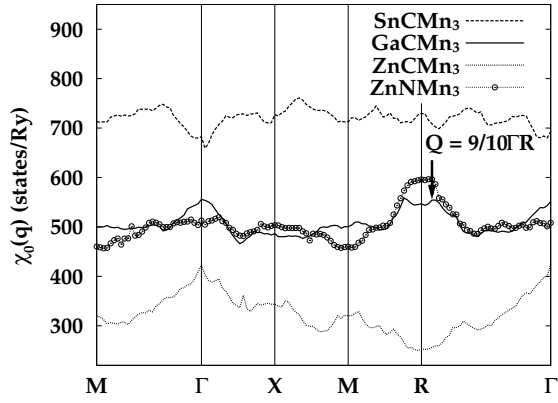


FIG. 3. The calculated susceptibilities of GaCMn₃ and related compounds. The vertical arrow denotes the local maximum of the susceptibility in GaCMn₃ with wave vector $\mathbf{Q} = \frac{9}{10}\Gamma\mathbf{R}$. SnCMn₃ and ZnCMn₃ are effectively one electron and hole doped compounds respectively, and ZnNMn₃ has the same number of valence electrons as GaCMn₃.

in Fig. 3 corresponds to the nesting vector $\mathbf{Q} (= \frac{9}{10}\Gamma\mathbf{R})$. Similar magnitudes of χ_0 at points Γ and \mathbf{R} indicates that both phases are competing.

For one-electron doped SnCMn₃, the susceptibility at point Γ is much suppressed, suggesting that the FM phase is unstable. This feature is consistent with the experiment. In the case of one-hole doped ZnCMn₃, the susceptibility at point \mathbf{R} is suppressed and local maxima are observed at other \mathbf{k} points including Γ . It would assist the appearance of complicated magnetic structures other than the AFM structure in the ground state. As for ZnNMn₃, the substantial enhancement of χ_0 is observed at point \mathbf{R} , whereas χ_0 at point Γ is suppressed. This feature is again consistent with the experimental result that the AFM phase is stabilized upon cooling without going through the FM phase.

We have also investigated electronic structures of GaCMn₃ both in the FM and AFM phases. Figure 4 shows the total DOSs of the FM and AFM phases GaCMn₃. In the inset of Fig. 4, total DOSs near E_F in both phases are compared. The high DOS in the PM phase is suppressed in the FM and AFM phases, which have 5.86 and 5.36 (states/eV) at E_F , respectively (Table I). It suggests that the FM and AFM phases are competing for the ground state. Total energy calculation indicates that the FM phase has lower energy than the AFM

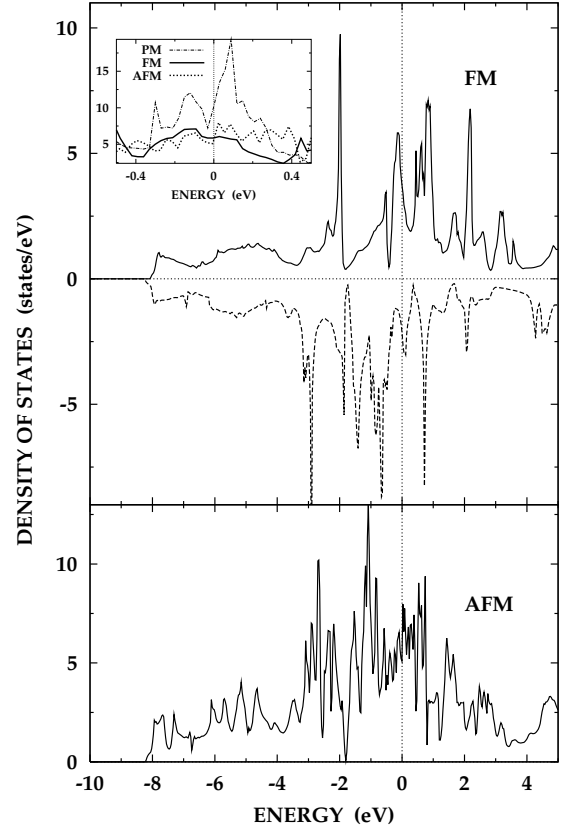


FIG. 4. Total DOSs of FM and AFM ground states of GaCMn₃. Inset compares the total DOSs of each magnetic ground states including the PM ground state near Fermi level.

phase by ~ 70 meV/GaCMn₃. Thus it does not seem to be consistent with the experimental result in which the AFM phase is the ground state, but such a small energy difference indicates that two phases are really competing and even the stable phase would be susceptible to external conditions such as temperature, pressure, magnetic field, and C stoichiometry.

To explore the effect of unit cell doubling in the AFM phase, the band dispersion along the $[111]$ direction is plotted in Fig. 5. For the comparison, the PM band structure calculated in the same doubled unit cell is also provided together (Fig. 5(a)). It is seen that the PM bands in the original sc unit cell are folded around the point P which corresponds to $\frac{1}{2}\mathbf{R}$ in the simple-cubic unit cell. Noteworthy is that two bands crossing the Fermi level along $\Gamma\mathbf{R}$ in the PM phase (represented by thick solid lines) are split by ~ 1.5 eV due to the unit cell doubling in the AFM phase. Thus, by band splitting, the DOS at E_F is reduced, and accordingly the AFM phase has effectively lower energy, which indeed is consistent with the nesting scenario mentioned above.

TABLE I. The calculated total and partial DOSs at E_F (in states/eV) and magnetic moments (in $\mu_B/\text{f.u.}$)

	N_{total}	N_{Ga}	N_{C}	N_{Mn}	μ_{total}	μ_{Ga}	μ_{C}	μ_{Mn}
PM	10.23	0.17	0.03	3.34				
FM	5.86	0.16	0.06	1.88	4.69	-0.12	-0.12	1.64
AFM	5.36	0.17	0.05	1.71	0.00	0.00	0.00	1.79

Table I provides magnetic moments in each magnetic phase. For the FM phase, the magnitude of Mn moment μ_{Mn} is $1.64 \mu_B$, whereas, for the AFM phase, $\mu_{\text{Mn}} =$

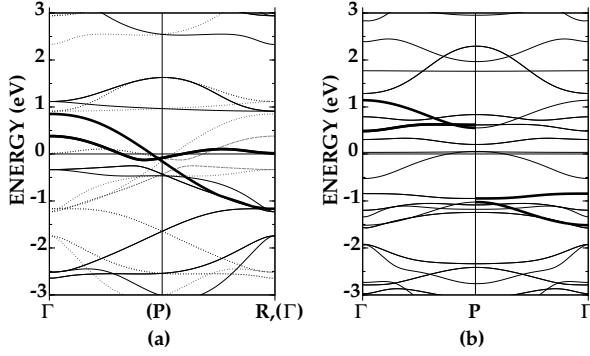


FIG. 5. (a) The band structure of GaCMn₃ along the [111] direction in the PM phase. The dotted lines represent the bands folded around the point P when the simple-cubic unit cell is doubled along the [111] direction. The thick solid lines correspond to the bands crossing the Fermi level. (b) The band structure of GaCMn₃ in the AFM phase along the line equivalent to (a). Note the bands of thick solid lines which are split by about 1.5 eV.

1.79 μ_B . The magnetic moment for the AFM phase is in good agreement with experiment [5] $\mu_{Mn} = 1.8 \mu_B$ at 4.2 K. As for the FM phase, $\mu_{Mn} = 1.64 \mu_B$ seems to be overestimated as compared to the experimental result $\mu_{Mn} = 1.3 \mu_B$ at 193 K. However, extrapolating the experimental value down to zero temperature would yield the magnetic moment close to the calculated one. To check the contribution of the orbital polarization to the magnetic moment, the LSDA+SO calculation including the spin-orbit interaction has been performed. We have found the negligible orbital magnetic moments $\sim 0.04 \mu_B/\text{Mn}$ in both phases, which is consistent with the itinerant nature of GaCMn₃.

In conclusion, we have performed the first principle electronic structure calculations on GaCMn₃ and related antiperovskite Mn compounds, SnCMn₃, ZnCMn₃, and ZnNMn₃. In the PM phase, GaCMn₃ shows the Fermi surface nesting with wave vector $\mathbf{Q} \sim \Gamma\text{R}$. The nesting feature is confirmed by the calculated susceptibility. Various magnetic structures of GaCMn₃ and related compounds are well explained by the wave vectors which give rise to the maximum susceptibilities. We have found that the DOS at E_F of AFM GaCMn₃ is similar to that of FM GaCMn₃ which results in the competing ground state phase. We have also demonstrated that the AFM GaCMn₃ is stabilized through the band folding effect. The orbital moment of Mn is found to be negligible, as expected in the itinerant magnetic system.

ACKNOWLEDGMENTS

This work was supported by the KOSEF through the eSSC at POSTECH and in part by the BK21 Project.

Helpful discussions with N.H. Hur and W.S. Kim are greatly appreciated.

-
- [1] K. Kamishima, T. Goto, H. Nakagawa, N. Minura, M. Ohashi, N. Mori, T. Sasaki, and T. Kanomara, Phys. Rev. B **63**, 024426 (2000).
 - [2] W. S. Kim, E. O. Chi, J. C. Kim, H. S. Choi, and N. H. Hur, Solid State Comm. **119**, 507 (2001).
 - [3] T. He, Q. Huang, A. P. Ramirez, Y. Wang, K. A. Reran, N. Rogado, M. A. Hayward, M. K. Haas, J. S. Slusky, Inumara, H. W. Zandbergen, N. P. Ong and R. J. Cava, Nature (London) **411**, 54 (2001).
 - [4] D. Fruchart, E. F. Bertaut, F. Sayetat, M. Nasr Eddine, R. Fruchart, and J. P. Senateur, Solid State Comm. **8**, 91 (1970).
 - [5] D. Fruchart and E. F. Bertaut, J. Phys. Soc. Jap. **44**, 781 (1978).
 - [6] T. Kaneko, T. Kanomata, and K. Shirakawa, J. Phys. Soc. Jap. **56**, 4047 (1987).
 - [7] D. Fruchart, E. F. Bertaut, B. Le Clerc, Le Dang Khoi, P. Veillet, G. Lorthioir, E. Fruchart, and R. Fruchart, J. Solid State Chem. **44**, 781 (1973).
 - [8] K. Kamishima, M. I. Bartashevich, T. Goto, M. Kikuchi, and T. Kanomata, J. Phys. Soc. Jap. **67**, 1748 (1998); K. Kamishima, T. Goto, T. Kanomata, and M. I. Bartashevich, J. Magn. Magn. Mater. **177-181**, 587 (1998); K. Kamishima, T. Goto, and T. Kanomata, Physica B **237**, 561 (1997).
 - [9] W. S. Kim, N. H. Hur, *et al.*, private communications.
 - [10] K. Motizuki and H. Nagai, J. Phys. C: Solid State Phys. **21** 5251 (1988).
 - [11] H. W. Myron, J. Rath, and A. J. Freeman, Phys. Rev. B **15**, 885 (1977). In our calculation, we have used an approximation of the constant oscillator strength matrix element M_{ij} .